Robotica (2018) volume 36, pp. 1188–1205. © Cambridge University Press 2018
doi:10.1017/S0263574718000334

Sliding mode control of a shape memory alloy actuated active flexible needle

Felix Orlando Maria Joseph†‡*, and Tarun Podder†

†*Department of Radiation Oncology, Case Western Reserve University, Cleveland, OH 44106, USA*
‡*Department of Electrical Engineering, IIT Roorkee, Roorkee, Uttarakhand 247667, India*

(Accepted April 07, 2018. First published online: May 7, 2018)

SUMMARY
In medical interventional procedures such as brachytherapy, biopsy and radio-frequency ablation, precise tracking through the preplanned desired trajectory is very essential. This important requirement is critical due to two major reasons: anatomical obstacle avoidance and accurate targeting for avoiding undesired radioactive dose exposure or damage to neighboring tissue and critical organs. Therefore, a precise control of the needling device in the unstructured environment in the presence of external disturbance is required to achieve accurate target reaching in clinical applications. In this paper, a shape memory alloy actuated active flexible needle controlled by an adaptive sliding mode controller is presented. The trajectory tracking performance of the needle is tested while having its actual movement in an artificial tissue phantom by giving various input reference trajectories such as multi-step and sinusoidal. Performance of the adaptive sliding mode controller is compared with that of the proportional, integral and derivative controller and is proved to be the effective method in the presence of the external disturbances.

KEYWORDS: Medical Interventions, Active Flexible Needle, Feedback Control

1. Introduction

Needles are one of the most significant minimally invasive tools to intervene diagnostic regions of the human body. In those needle-based therapeutic percutaneous, medical interventional procedures such as biopsy, fluid/blood collection, brachytherapy, radio-frequency-based thermal ablation, cryotherapy, anesthetic drug delivery, neural stimulation and so on,[1] accurate needle placement is one of the major requirements, as the success of such procedures are dependent on the accuracy of the needle placement. To enhance needle steerability while performing the percutaneous interventions, Webster III *et al.*[2] have proposed a methodology that entails precurved concentric tubes with stiffness variation. A further approach to execute improved needle steerability with minimal tissue damage and higher curvature, is proposed by Swaney *et al.*,[3] which features a flexure-based kinked needle design.

The flexible needle steering techniques are categorized mainly into passive needle steering and active needle steering. The passive needles are the ones which have no actuators and sensors attached to their shaft. Rather, they are mere free bodies either with symmetrical or asymmetrical tip to undergo the reaction force from the tissue environment.

1.1. Passive needle steering

Conventionally, these needles are steered through base manipulation, through which lateral translations and rotations are applied to the base of the needle. Due to the lateral movement of the needle inside the tissue region, the needle gets deflected and hence it is possible to control the trajectory on the needle tip. In order to avoid large forces applied on the tissue, especially during deep insertions, tip steering method is used. In this method, the lateral forces created at the tip of the needle are used for steering. By rotating the flexible bevel tip needles around its shaft and pushing it in the forward direction, the

* Corresponding author. E-mail: felixfee@iitr.ac.in
E-mail: txp172@case.edu

https://doi.org/10.1017/S0263574718000334 Published online by Cambridge University Press

target can be reached by pointing the bevel toward the target. However, the radius of curvature is more difficult to control, as it depends upon the relative difference between the needle and the tissue and also the geometry of the bevel tip (bevel angles of 30° and 45°). Thus, the passive bevel tip flexible needles require the needle tissue interaction model to control the needle-path curvature. The needle tissue interaction can be modeled using, empirical models,[4] finite element models,[5–7] beam theory with local virtual springs[8] and fracture-mechanics-based analytical models[9] for predicting needle force and its relationship with surrounding boundary conditions, insertion velocity and body geometry.

Several researchers have worked extensively on the passive flexible needle steering methodology. Reed *et al.*[10,11] presented an optimal steering system integrating patient specific 2D preoperative planning. Similarly, Alterovits and Goldberg[12] have presented the intraoperative planning for the flexible needle steering. In the control aspect, Kallem and Cowan[13] have proposed a feedback linearization-based planar motion controller for the flexible needle involving rotation and insertion inputs. Furthermore, torsion compensation during the passive flexible needle steering is performed by.[14] Several other researchers such as Wood *et al.*,[15,16] Ko and Rodriguez y Baena[17] through duty-cycle rotation-based non-linear control and model predictive control, respectively, have worked on the trajectory following control of the flexible needles. More recently, Bui *et al.*[18] have presented a novel curvature controllable needle with enhanced needle steerability. In their proposed needling system, the torsional friction force is reduced during tissue contact, by lowering the needle's whole-body rotation, thereby assuring reduction in the tissue damage. All these works were focusing on static workspace-based needle trajectory regulation. However, the preplanned trajectory-based planning and control approach may not be successful in the clinical environment due to the dynamic environment existence which involves patient limb motion and breathing, by which the target will be changing instantaneously. To address this challenge, Hauser *et al.*[19] have used the adaptive control loop planning for needle steering, concerning the changes in the target. Later, Abayazid *et al.*[20] and Patil *et al.*[21] have also worked on the flexible needle steering considering the dynamically changing environment through integration of image feedbacks and needle deflection models and rapid replanning to reach 3D targets, respectively.

The main limitations in passive needle steering techniques include, more number of needles puncturing the target region, less conformity, actuation from the base only, limited sensory feedback and unavoidable exposure of neighboring tissues to radioactive dose in the case of brachytherapy.

1.2. Active needle steering

From the research study so far in the flexible needle-based interventional procedures, it is observed that accurate placement of needle in the specified target is quite challenging. For example, in prostate brachytherapy, the accurate needle placement is critical and challenging because of the necessity to avoid the neighboring organs—rectum, bladder, penile bulb, neurovascular bundle and urethra so that they are not exposed to undesired radiation dose. Podder *et al.*[22] have reported that needle geometry and lack of proper actuation of the needle are the major reasons for this challenge. By proposing a novel curvilinear method of approaching the given target, they have shown a significant reduction in both the total number of needles employed and the amount of radiation dose to the bladder, urethra and rectum during prostate brachytherapy.

An active flexible needle is required to accomplish the task of following a curvilinear path avoiding anatomical obstacles and critical organs while reaching the target. Poddet *et al.*[23] have also proposed an active needle concept with body attached smart actuators by providing bending forces to enhance needle tip placement accuracy and thereby ascertaining improved clinical outcome (Fig. 1). The clinical advantages of the active needle with external actuation and control over the conventional passive bevel tip needles include (i) enabling the surgeons and clinicians to correct the previously achieved misalignments in reaching the target with the conventional passive needles, (ii) damage avoidance to critical organs and anatomical organs during insertion because of self-actuating capability of the smart active needles, (iii) trauma minimization to the patients by potential decrease of number of needle insertions (Podder *et al.*[22,23] and Stock *et al.*[24]).

In contrast to the passive needle steering techniques, the active mechanism-based smart needles which have the self-actuating capability, require no needle–tissue interaction model for the needle–path curvature control. During the steering of active needles, the whole shape or the needle tip or the cannula conforms to the share and geometry of the organ of target.[23] Also, the active needle has high complexity in their design mechanism in comparison to the passive needling system. The active

https://doi.org/10.1017/S0263574718000334 Published online by Cambridge University Press

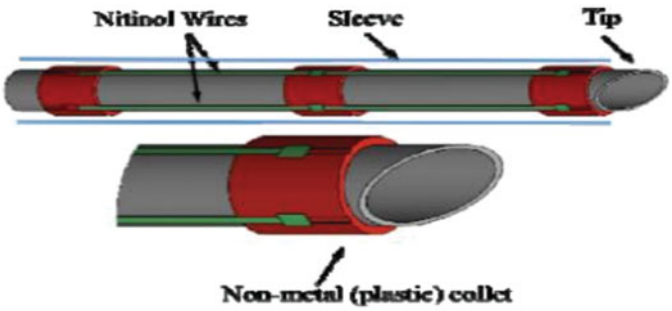


Fig. 1. Conceptual schematic of active needle.[23]

needles can be categorized as active cannulas, precurved stylets, tendon-actuated active tips and shape memory alloy (SMA) wire actuated needles.

A multiple precurved concentric tubes based active cannula was presented by Webster *et al.*,[25] which by means of simultaneous rotation and extension of the concentric tubes with respect to each other, could achieve adaptable cannula curvature, tip position and tip orientation. A detailed study on tube pairs balancing is done by Sears and Dupont[26] and Reed *et al.*[27] in active needle steering. For these active cannulas, tissue environmental contact force is not needed for actuation, as the cannula itself is of self-actuating capability. However, these balanced tube pairs are not suitable for dynamic environments. The extensive study on torsion in balanced active cannula models is done by Reed *et al.*,[28] Swensen *et al.*[29] and Burdette *et al.*[30]. Then, it has to be noted that, Burgner *et al.*[31] are the first research group to work with active cannula steering utilizing ultrasound ablation in ex-vivo tissue. Various other designs of active cannulas are proposed by Levy *et al.*[32] and Furusho *et al.*[33]

Tendon actuated active tip-steering methodologies are currently being used in endovascular guidelines[34] and laparoscopic tools.[35] In needle steering methodology, this approach of tendon based actuation is implemented by connecting the tip to the needle body or stylet though a mechanical joint (spherical joint) or through a flexible element such as nylon connector. By proving the actuation through the tendon cables, the tip will be bent accordingly. In general, the cannula and stylet will have grooves to accompany the cable path and sensor placement (optical fibers). Henken *et al.*[36] have performed closed-loop steering experiments in phantom tissue using PI controller through FBG-based reconstruction of the needle shape. Adebar *et al.*[37] have also performed the tendon based needle steering using an articulated rotational joint. These active needles find wide application in transthoracic lung biopsy, musculoskeletal percutaneous injection and aspiration procedures including biopsy.[38,39]

Though the tendon driven needle steering shows good outcome, the following limitations exist in these procedures.

1. High stiffness of the needle suffers during deep tissue insertion.
2. Cost-effective due to the mechanical complexity of the needle interior design (having grooves and slits for tendon lining to the tip and fiber sensor placements).

To overcome these challenges in the tendon actuated needle steering procedures, very recently, Yamada *et al.*,[40] have proposed an active sheath based novel steering mechanism. They have performed only 2D needle steering where the 3D based work is their future scope.

Flexinol SMA wire with the unique characteristics of biocompatibility, super-elasticity, high power to weight ratio and shape memory effect is successfully used as the smart actuator for the active needle.[41] In the SMA wire actuator, a phase transition from low-temperature martensite phase to high-temperature austenite phase due to the thermal activation by passing electric current to the SMA wire actuator, can generate actuation force in it. The prime merits of SMA actuated active needle over conventional rotating bevel tip passive needle include (i) high needle body deflection achievement, (ii) needle–tissue interaction without plastic deformation.[41–46] Considering these merits, Ryu *et al.*[41] have proposed an optically controlled MR compatible active flexible needle equipped with a silica optical fiber with standard FBGs for temperature sensing and a plastic optical fiber for needle shape bending measurement, so that closed loop control of the needle can be performed using the Auricchio algorithm-based elastic model. Konh *et al.*[42–44] and Datla *et al.*[45,46] have performed extensive work on

https://doi.org/10.1017/S0263574718000334 Published online by Cambridge University Press

the SMA actuated active needle design and development and the modeling of needle tissue interaction, respectively.

Several researchers including our group are working on the design, modeling and control of active flexible needles for percutaneous medical interventions.[47–54] As the work presented here is on the control of an active flexible needle, the literature survey following next is focused specifically on the control of active flexible needles.

Ayvali *et al.*[47] have developed and evaluated the performance of a novel multi-degrees of freedom (DOF) SMA actuated cannula using pulse width modulation control strategy, in a switched mode position control with visual and temperature feedbacks. Ruiz *et al.*[48] have performed a closed-loop control of an SMA actuated active flexible needle in air and in water experimental conditions with EM sensory feedback at different sampling rates using proportional, integral and derivative (PID) and PID-P^3 controllers. Ko *et al.*[49] have proposed the "programmable bevel" concept for probe steering using EM sensor-based feedback control through a state feedback control scheme namely approximate linearization technique. Xu *et al.*[50] have presented a configuration comparison for kinematic performances among three optimized continuum manipulators for the development of single access point robotic surgeries. Their results could serve as the reference for the development of surgical robots with one point access and continuum mechanisms in the medical robotics field. Maria Joseph *et al.*[51] have tested the trajectory tracking performance of the SMA actuated flexible needle using three feedback modalities such as EM, vision and US. They have found that the trajectory tracking performance with EM sensory feedback modality shows smaller root mean square error (RMSE) compared to that with the vision and US feedbacks. In addition, they have performed a coordinated closed-loop control strategy of a robot guiding an SMA actuated active flexible needle in curvilinear trajectory tracking task. The robot control loop is considered as the outer loop and the flexible needle loop forms the inner one (Maria Joseph *et al.*[52–54]). Recently, they have performed the closed-loop inverse kinematic control of a smart 2-DOF active needle to track the given 3D trajectory.[55] They have validated their proposed controller with in-air experiments using stereo vision feedback with depth information along with simulation studies. Their main future aim is to optimize the dimension of the active needle to the standard 16G brachytherapy needle for percutaneous interventions. Van de berg *et al.*[56] have presented an actively controllable tip steerable needle with actuation using a tendon material and FBG-based shape sensing and tip location detection. They are the first to perform active needle steering using FBG-based shape feedback. In their study, a generic PI controller with same gains have been used for the entire tip orientations. For the first time, a sliding mode controller for steerable needle interventions in tissue environment under the imaging feedback modality is proposed by Rucker *et al.*[57] However, the needle utilized in their work is a bevel tip flexible needle which is actuated only at its base through insertion and rotational velocities.

The prospect of needle steering will rely on the advancement of mechanically robust needle design, suitable control algorithms and high-quality system feedback.[52–54] From Swaney *et al.*,[3] it is acknowledged that there has been a great progressive deal in the design and system feedback strategies, little focus has been done toward the adaptive control of active needles. In percutaneous medical interventions with the SMA actuated active flexible needles, several factors such as the needle–tissue interaction, sensory feedback and SMA non-linearities could affect the tracking accuracy within the tissue medium. From the knowledge of the authors of the present work, so far in the literature, no one has performed the trajectory tracking control of the SMA actuated active flexible needle using adaptive PID sliding mode controller (APID-SMC) to verify the robustness against the disturbance due to SMA non-linearities and tissue reaction force. This motivates the authors to perform the closed-loop control of the SMA actuated active flexible needle using adaptive sliding mode controller. Furthermore, the robustness of the applied APID-SMC is tested under two disturbance analyses. First, by forced convection of the SMA wire actuator, thermal disturbance is applied at various time instants by blowing air on the actuator. Second, by diverting the movement of the needle tip using a force/torque sensor equipped rod, various external point load disturbances are applied at random time instants of the tip movement.

Thus, in this current work, we have applied the non-linear adaptive sliding mode controller for obtaining a precise, disturbance overcoming performance during the trajectory tracking task of the SMA actuated active flexible needle in tissue mimicking soft material (Plastisol, M-F Manufacturing, Fort Worth, TX) phantom. By changing the compositions of plastic (polyvinylchloride suspension) and softener, the elastic modulus of the phantom can be modified accordingly. In our study, the

https://doi.org/10.1017/S0263574718000334 Published online by Cambridge University Press

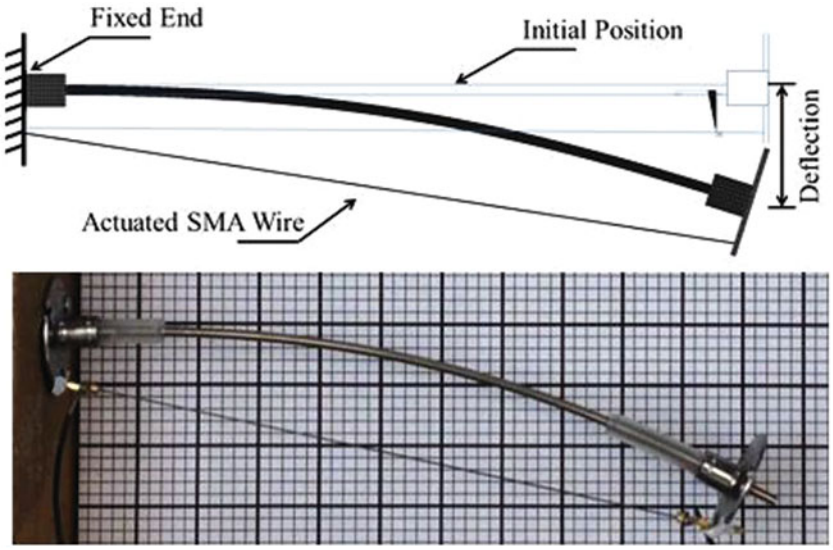


Fig. 2. Deflection model of the experimented active needle.[44]

plastisol phantom was prepared with 3:1 ratio of plastic to softener. The material properties of the phantom are discussed in Datla *et al.*[45]

The rest of the paper is organized as follows. In Section 2, the methodologies involved in this work are presented. This section will briefly present the description of the SMA actuated active flexible needle system, design of the adaptive PID sliding mode control (APID-SMC) and the experimental setup. Section 3 presents the experimental results. Then, the results are discussed in Section 4. Finally, concluding remarks are provided in Section 5.

2. Methods

2.1. Needle deflection model

The SMA wire actuated needle deflection model is performed using finite element analysis by our research collaborators (Kohn *et al.*[44]).

At the proximal end of the needle, the SMA wire actuator is connected using two discs as shown in Fig. 2. In order to avoid the interaction of the actuator inside the tissue during the needle maneuverability, the actuation part is kept at the proximal end of the needle. The needle bends due to the contraction of the SMA wire upon conventional Joules heating by passing electric current in the range of 0–1 A. The movement of the tip is proportional to the SMA wire actuation as there is no separate flexure-based connection between the needle body and the tip. The whole needle is a single body whose dimensions are given in Section 2.4 while describing the experimental setup.

2.2. System description

The second-order system dynamics of the SMA actuated active flexible needle is given by

$$\begin{aligned} \dot{x}_1(t) &= x_2(t) \\ \dot{x}_2(t) &= f(x_1, x_2, t) + \Delta f(x_1, x_2, t) + b(x_1, x_2)\, u + d(t) \\ y &= x_1(t) \end{aligned} \tag{1}$$

where $x_1(t)$ and $x_2(t)$ are the system states representing the position and velocity of the SMA actuator, respectively, u and y are the control input and system output, respectively, $b(x_1, x_2)$ is the input gain, $f(x_1, x_2, t)$ and $\Delta f(x_1, x_2, t)$ are the system nominal parameter and uncertainty, respectively. $d(t)$ represents the external disturbance. As per assumption, $\Delta f(x_1, x_2, t)$ and $d(t)$ are bounded by two parameters, α and g such that the conditions, $|\Delta f(x_1, x_2, t)| \leq g$ and $|d(t)| \leq \alpha$ are satisfied. It is also assumed that the input gain, $b(x_1, x_2)$ is bound to be within the range $b_{\min} \leq b \leq b_{\max}$.

https://doi.org/10.1017/S0263574718000334 Published online by Cambridge University Press

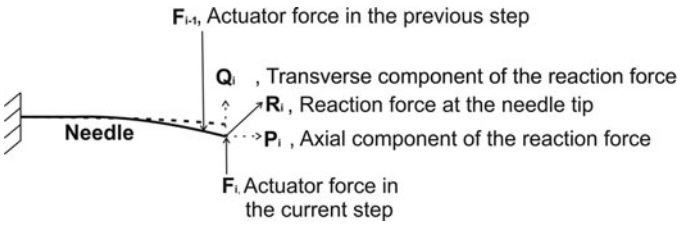


Fig. 3. Illustration showing the forces acting on the needle at every increment of i. R_i, Q_i and P_i are the reaction force at the tip of the needle and its transverse and axial components, respectively.

2.3. Mechanics of the needle–tissue interaction

In our study, we have considered only the needle's deflection and no insertion is considered. Hence, the energy-based model which describes the mechanics of the needle–tissue interaction will include only needle deflection. Furthermore, the frictional forces acting on the needle were not considered because of the negligible effect on the needle deflection.

The total system energy in this model is expressed in terms of transverse, $t(x)$ and axial, $a(x)$ needle deflections. Using Rayleigh–Ritz method, the coefficients of the functions forms (initially assumed) for the needle deflection functions have been found. The system energy Φ, is calculated by considering the internal energy U, stored in the system and the work done W by the system as

$$\Phi = U - W \tag{2}$$

The initial energy, U is composed of the energy stored by the needle bending B_E and the energy of the tissue deformation, D_E.

These B_E and D_E are given by

$$B_E = \frac{\mathrm{EI}}{2}\int_0^{l_i}\left(\frac{d^2 t_{i-1}}{dx^2}\right)^2 \mathrm{d}x + \frac{\mathrm{EI}}{2}\int_0^{l_i}\left(\frac{d^2\,(t_{i-1}-t_i)}{dx^2}\right)^2 \mathrm{d}x + \frac{\mathrm{EA}}{2}\int_0^{l_i}\left(\frac{da_{i-1}}{dx}\right)^2 \mathrm{d}x + \frac{\mathrm{EA}}{2}\int_0^{l_i}\left(\frac{\mathrm{d}(a_i - a_{i-1})}{dx}\right)^2 \mathrm{d}x \tag{3}$$

$$D_E = \frac{1}{2}\int_0^{l_i} K_T (t_i - t_{i-1})^2 \mathrm{d}x + \frac{E_T (\mathrm{A} l_i)^2}{3\,(1-2\gamma_T)} \tag{4}$$

where the subscripts i and $i-1$ denote the present and previous iterations. E, I, A and l are the elastic modulus, moment of inertia, cross-section area and the length of the needle, respectively. K_T and γ_T are the stiffness and Poisson's ratio of the tissue.

Work done on the system include the work of actuation, W_{actuator}, expressed as

$$W_{\text{actuator}} = C^n_{\text{actuator}}(t_i\,(x_m) - t_{i-1}\,(x_m) + C^a_{\text{actuator}}\,(a_i\,(x_m) - a_{i-1}\,(x_m)) \tag{5}$$

where C^n_{actuator} and C^a_{actuator} are the normal and axial actuator forces acting at the location x_m of the needle.

As shown in Fig. 3, the needle tip reaction force R_i, is resolved into transverse, Q_i and axial, P_i components.

The corresponding work done by these components are given by

$$W_Q = Q_i\,(t_i\,(l_i) - t_{i-1}\,(l_i)) \tag{6}$$

$$W_P = P_i\,(a_i\,(l_i) - a_{i-1}\,(l_i)) \tag{7}$$

https://doi.org/10.1017/S0263574718000334 Published online by Cambridge University Press

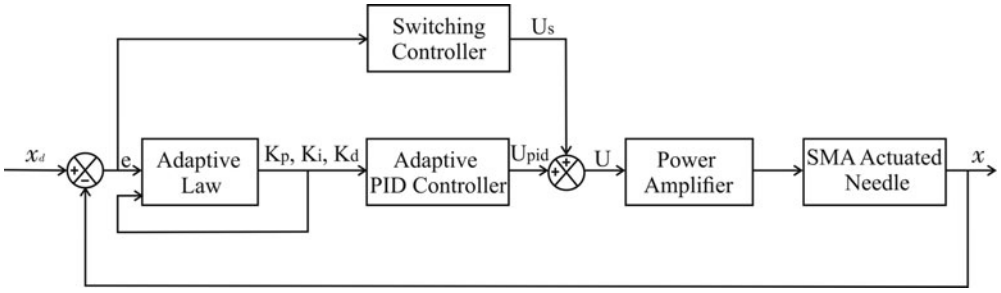


Fig. 4. Block diagram of the adaptive PID sliding mode control.

where W_Q and W_P are the works done by the reaction forces Q_i and P_i, respectively. Furthermore, the work done in rupturing the tissue W_R is given by

$$W_R = g\, T_r a_i\,(l_i) \tag{8}$$

where T_r is the rupture toughness, g is the rupture width and $a_i(l_i)$ is the rupture length. Thus, the above equation is the product of these three parameters.

2.4. Design of the adaptive PID sliding mode controller

The APID-SMC block diagram is shown in Fig. 4. Let the error between the given desired trajectory y_d and the system output y is represented by

$$e = y_d - y \tag{9}$$

For having second-order error dynamics, a new reference signal, x_r can be defined as

$$\dot{x}_r = \ddot{y}_d + K_1\dot{e} + K_0 e \tag{10}$$

where K_1 and K_0 are chosen by the control designers such that the roots of the characteristic equation $s^2 + K_1 s + K_0 s = 0$ lie in the open left half of the complex plane.

The sliding surface function σ is defined such that the system behaves unvaryingly as a linear system when in the sliding mode. Let the sliding function be defined as

$$\sigma = x_r - x_2 \tag{11}$$

During sliding mode occurrence, the sliding function σ become 0, which implies, $x_r = x_2$ or $\dot{x}_r = \dot{x}_2$. By equating Eq. (10) and the expression $\dot{x}_r = \dot{x}_2$, we get

$$\ddot{e} + K_1\dot{e} + K_0 e = 0 \tag{12}$$

Thus, Eq. (12) implies that the trajectory tracking error e goes to zero as time tends to infinity. Using Eqs. (9) and (10), the sliding surface σ, given by Eq. (11), can be rewritten as

$$\sigma = \dot{e} + K_1 e + K_0 \int e\mathrm{d}t \tag{13}$$

Thus, from Eq. (13), it is observed that integral sliding surface is achieved because of the new reference signal x_r and the control performance can be increased as the sliding surface converges to zero by the presence of the integral element.

For achieving, the system stability, the control input, u is chosen so that it satisfies the condition,

$$\dot{\sigma} = -K\,\mathrm{sat}\,(\sigma) \tag{14}$$

https://doi.org/10.1017/S0263574718000334 Published online by Cambridge University Press

where

$$\text{sat}\,(\sigma/\delta) = \begin{cases} 1 & \sigma/\delta > 1 \\ -1 & \sigma/\delta < -1 \\ \sigma/\delta & \text{others} \end{cases}$$

Taking derivative of Eq. (11) and substituting Eq. (1), we obtain the derivative of the sliding surface as

$$\dot{\sigma} = (\dot{x}_r - (f(.) + \Delta f(.) + b(.)\,u + d)) = -K\text{sat}\,(\sigma) \tag{15}$$

From Eq. (15), the control input u is computed as

$$u = \frac{1}{b}\left[K\text{sat}\,(\sigma) + \dot{x}_r - (f(.) + \Delta f(.) + d)\right] \tag{16}$$

In general, the control input shown in Eq. (16) is divided into two parts as follows:

$$u = u_s + u_{\text{eq}} \tag{17}$$

where $u_s = \frac{1}{b}[K\text{sat}(\sigma)]$ is the supervisory controller which guarantees stability of the system by switching the system to the sliding mode surface and $u_{\text{eq}} = \frac{1}{b}[\dot{x}_r - (f(.) + \Delta f(.) + d)]$ is the control at the equivalent point, which makes the system states stay on the sliding surface (Kuo *et al.*[58]).

The adaptive PID tuning controller is used for approximating the unknown and uncertainty parameters in the equivalent control, u_{eq}. As the adaptive PID tuning controller undertakes the equivalent control well by generating the control signal even in the case of hysteresis and disturbance (Tai and Ahn[59]), it is ensured that the sliding surface goes to zero and hence, the chattering problem prevalent in sliding mode control is suppressed. Thus, we consider the following equation:

$$u_{\text{eq}} \approx u_{\text{PID}} = K_P e + K_I \int e\,\mathrm{d}t + K_D \dot{e} \tag{18}$$

Then, the adaptive laws for the PID control gains, K_P, K_I, K_D based on the gradient descent method are given by

$$\begin{aligned} K_P(k+1) &= K_P(k) + \gamma_1 \phi e \\ K_I(k+1) &= K_I(k) + \gamma_2 \phi \int e\,\mathrm{d}t \\ K_D(k+1) &= K_D(k) + \gamma_3 \phi \dot{e} \end{aligned} \tag{19}$$

As u_{PID} becomes equal to u_{eq}, ϕ equals zero, and so $\sigma \to 0$. Hence, Eq. (19) can be further restructured as

$$\begin{aligned} K_P(k+1) &= K_P(k) + \gamma_1 \sigma e \\ K_I(k+1) &= K_I(k) + \gamma_2 \sigma \int e\,\mathrm{d}t \\ K_D(k+1) &= K_D(k) + \gamma_3 \sigma \dot{e} \end{aligned} \tag{20}$$

2.5. Experimental setup

The experimental setup for steering a SMA actuated active flexible needle in an artificial tissue mimicking phantom is shown in Fig. 5.

The actual needle tip position is obtained by a 5DOF electromagnetic (EM) tracking sensor (Aurora, Northern Digital Inc., Waterloo, Ontario, Canada[60]) at a sampling period of 1 ms. Figure 6, depicts the zoomed-in view of the SMA wire actuated active flexible needle prototype employed in our experiment.

The overall experimental system parameters are listed in Table I.

As shown in Fig. 6, the EM sensory insulated coil is attached to the needle tip. The actual position of the needle tip is referenced with respect to the global reference frame considered at the top center of the EM field generator. The interface between the active flexible needle's power amplifier circuit

https://doi.org/10.1017/S0263574718000334 Published online by Cambridge University Press

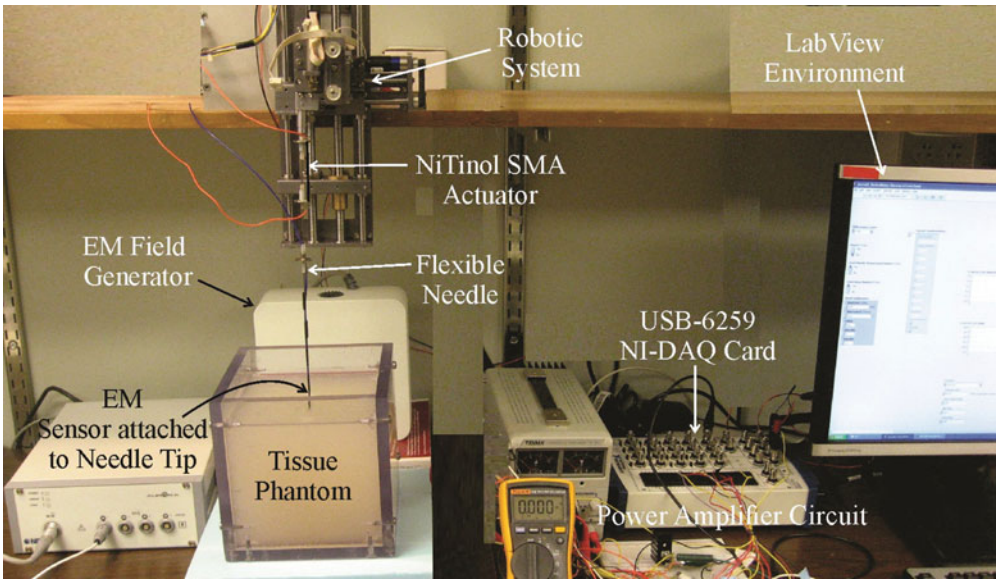


Fig. 5. Experimental setup.

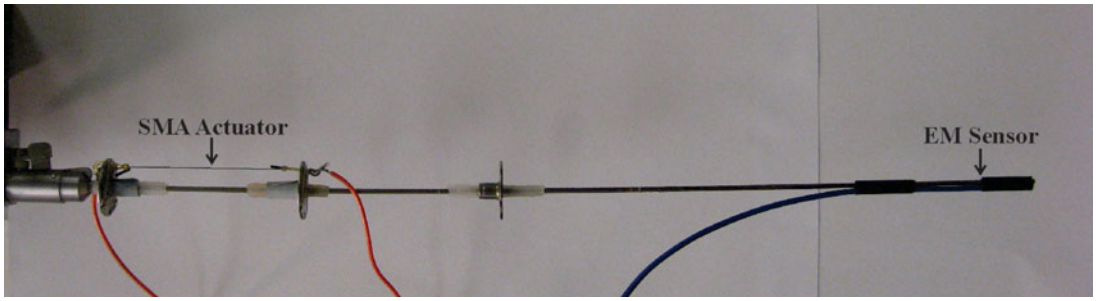


Fig. 6. Zoomed view of the SMA actuated active flexible needle.

and the control computer is supported by the NI-DAQ card (USB-6259, 16-bit, 250 KHz operating frequency and 0.03% accuracy). Through LabView (NI, Dublin, Ireland) programming environment, the control commands are generated using the adaptive PID sliding mode algorithm implemented in a Pentium IV, 32-bit, 2 GB RAM and 2.8 GHz speed hard shield experimental computer.

3. Results and Discussions

The prime objective of this piece of work is to apply the adaptive control algorithm to an active smart flexible needle for percutaneous cancerous interventions to enhance the steering capability from the viewpoint of clinical environment. From the previous study of the authors,[51–54] it is observed that EM sensory feedback provides greater accuracy in proving the actual position of the needle during insertion in tissue. Thus, in this study, we have utilized the same EM sensory feedback in comparison to the imaging modality, which suffers in giving the accurate values of the tracked needle. The results obtained from the real-time experiments are shown and discussed in this section. The experiments are performed first with multi-step input reference for the needling system to track in the artificial tissue phantom. The quantitative performance measure of the controller in performing the robot control in guiding the needle to track the desired trajectory is performed by computing the RMSE between the desired and the actual trajectories. The RMSE between the desired and the actual trajectories is given by

$$E_{\mathrm{RMSE}} = \sqrt{\frac{1}{N}\sum_{i=1}^{N}\left[x_{\mathrm{des}}\,(i) - x_{\mathrm{act}}\,(i)\right]^2} \tag{21}$$

https://doi.org/10.1017/S0263574718000334 Published online by Cambridge University Press

Table I. List of experimental device parameters.

Device	Main parameters
Active flexible needle	Mass: 20 g Material: aluminium Length: 200 mm Diameter: 1.70 mm
SMA actuator	Make: flexinol Type: nitinol pull actuator Length: 70 mm Diameter: 0.25 mm Heating pulling force: 891 g Cooling deformation force: 356 g Resistance: 1.3 Ω
NI-DAQ card	Make: national instruments Type: USB-6259 Operating frequency: 16 KHz Accuracy: 0.03% 16 bit card
Power amplifier	IC: LM324AN Output: 0 – 1 A Input: 0 – 10 V
EM sensor system	Make: northern digital inc. DOF: 5 Connection: serial Port Position accuracy: 0.6 mm Position precision: 0.4 mm Position trueness: 0.5 mm

where N is the total number of way points of the trajectory, i is the discrete value and $x_{\text{des}}(i)$ and $x_{\text{act}}(i)$ are the respective ith desired and actual values.

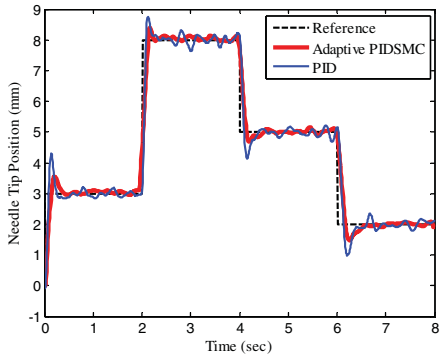
For repeatability analysis purpose, a set of five readings are taken for the same input reference. Figure 7 shows the control results with respect to the multi-step reference input. The APID-SMC parameters are set as

Sliding surface parameters: $K_0 = 1$; $K_1 = 25$;
PID Learning rates: $\gamma_1 = 0.5$; $\gamma_2 = 1.5$; $\gamma_3 = 0.8$;
Supervisory control parameters: $K = 0.8$; $\delta = 0.4$;
Similarly, the PID parameters are set as: $K_P = 1$; $K_I = 20$; $K_D = 0.001$.

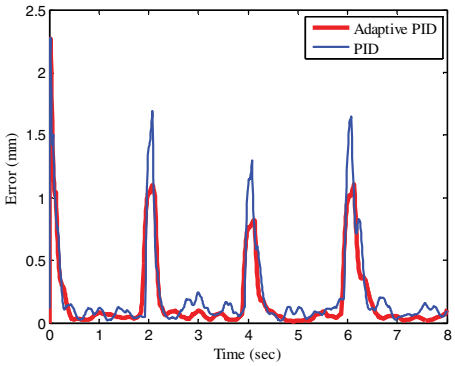
Comparison of system tracking performance between APID-SMC and PID controllers is presented in Fig. 7(a). The APID-SMC shows much smoother and less overshooting response compared to that of the PID controller. For this particular run (among the five repetitive runs), the RMSE values for APID-SMC and PID controller are 0.63 mm and 0.74 mm, respectively. Figure 7(b) shows the error norm plot corresponding to the reference matching plot. As shown in Fig. 7(b), the error norm for APID-SMC-based tracking is of minimum magnitude (closer to zero) as compared to the error norm of PID. The adaptive tuning of the individual gain parameters (K_P, K_I and K_D) as per the Eq. (13) are shown in Fig. 7(c) to 7(e), respectively. The orders of $K_P(k)$, $K_I(k)$ and $K_D(k)$ are $O(10^{-1})$, $O(10^{1})$ and $O(10^{-3})$, respectively. Similarly, the sliding surface function value given by Eq. (7), throughout the tracking task is shown in Fig. 7(f). Finally, Fig. 7(g) and 7(h) show the control input voltage signals to the SMA actuator driving the active flexible needle by applying APID-SMC and PID controllers, respectively. The control voltage is hard limited within the range of 0–10 V, as it is supplied via the NI-DAQ card to the needle power amplifier circuit (please see Appendix). For APID-SMC, the control voltage ranges between 2.2 V and 7.0 V, whereas with PID controller application, the complete range (0–10 V) has been attained.

Next, with the same set of APID-SMC and PID control gain parameters, the experiments are performed with sinusoidal control reference with the frequency of 2 Hz. The corresponding control

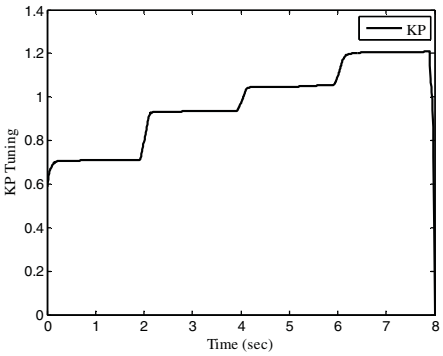
https://doi.org/10.1017/S0263574718000334 Published online by Cambridge University Press



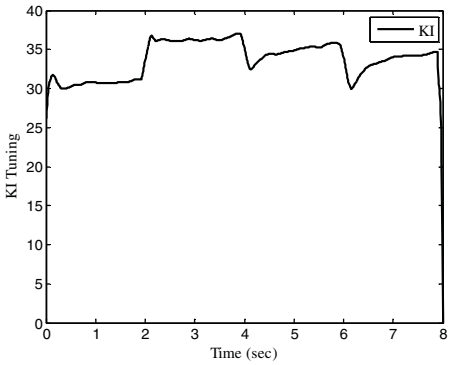
(a) Comparison of APID-SMC and PID controller in tracking the given multi-step reference.



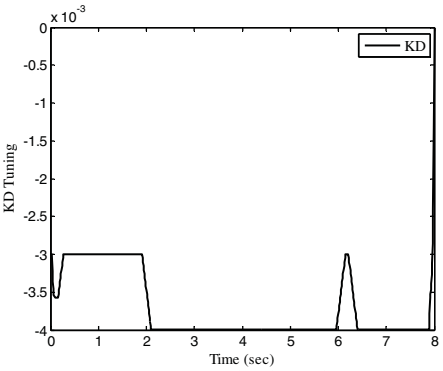
(b) Error plot



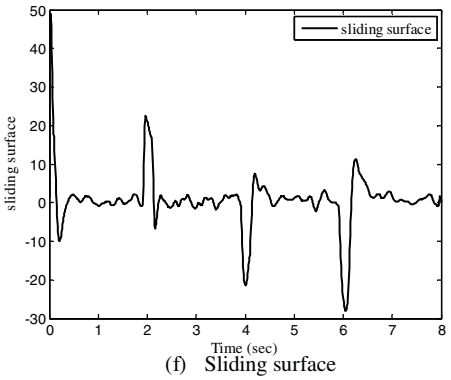
(c) Adaptively tuned proportional gain K_P



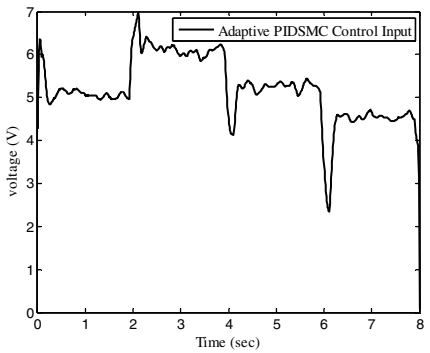
(d) Adaptively tuned Integral gain K_I



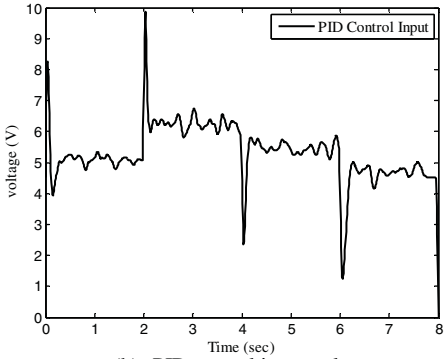
(e) Adaptively tuned derivative gain K_D



(f) Sliding surface



(g) APID-SMC control input voltage



(h) PID control input voltage

Fig. 7. Control performance with the given multi-step reference. (a) Comparison of APID-SMC and PID controller in tracking the given multi-step reference. (b) Error plot. (c) Adaptively tuned proportional gain K_P . (d) Adaptively tuned Integral gain K_I. (e) Adaptively tuned derivative gain K_D . (f) Sliding surface. (g) APID-SMC control input voltage. (h) PID control input voltage.

https://doi.org/10.1017/S0263574718000334 Published online by Cambridge University Press

Table II. RMSE comparison.

Controller	Multi-step reference (Mean ± SD in mm)	Sinusoidal reference (Mean ± SD IN MM)
Adaptive PID-SMC	0.85 (±0.10)	0.75 (±0.09)
PID	0.98 (±0.07)	0.92 (±0.08)

results for the given input sinusoidal reference trajectory is shown in Fig. 8. Similar to the multi-step reference-based experiment, here too five set of reading are taken for the repeatability analysis. As the trajectory is continuous in nature, there exist smaller overshoot as compared to the multi-step reference performance results. The RMSE values for the sinusoidal tracking task by applying APID-SMC and PID are 0.84 mm and 0.99 mm, respectively, for this particular run. The adaptation of the PID gains of the APID-SMC controller are shown in Fig. 8(c) to 8(e), respectively. $O(10^{-1})$, $O(10^{1})$ and $O(10^{-3})$, are the APID-SMC control gain orders, respectively. Similarly, the sliding surface function trajectory, and the control input voltages are shown in Fig. 8(f) to 8(h), respectively. Table II shows the statistical results of the APID-SMC and PID controller performance in terms of the RMSE values. From this quantitative analysis, it is observed that, the APID-SMC exhibits better control performance for the given trajectory input commands. As mentioned in the introduction section that the main purpose of applying APID-SMC is to overcome the effect of external disturbance while tracking the given desired input trajectory. The robustness of the SMA actuated active flexible needling system is checked under two different tests. First, by forced convection of the SMA wire actuator, thermal disturbance is applied at various time instants by blowing air on the actuator. As shown in Fig. 9, the extended portion of the needle (distal end) is inside the artificial phantom and the air is blown (at random intervals) on the SMA actuator which is affixed near the proximal end of the needle. The controller applies more voltage due to the loss of heat caused by the disturbance thereby, establishing the required temperature of the SMA actuator. Figure 10 shows the performance of the APID-SMC despite the influence of external disturbance due to forced convection of the SMA actuator. The box marked regions (Fig. 10(a)) are the ones where SMA actuator has undergone forced convection as disturbance to the needling system. From Fig. 10(a), it is clearly observed that the deviation in the tracking trajectory due to the external disturbance can be overcome by the controller in tracking back the given sinusoidal trajectory soon after the disturbance. Figure 10(b) shows the corresponding change in the control input voltage.

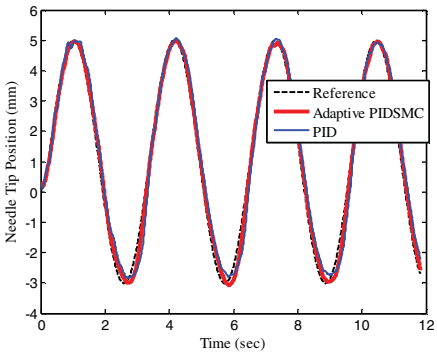
Similarly, the second test in checking the robustness of the control system is performed by applying various external point load disturbances at random time instants of the tip movement. An elongated rod equipped with Nano17-10173 Force/Torque sensor (ATI Industrial Automation[61]) is used for this purpose. Figure 11 depicts clearly that the external force disturbance is applied to the needle tip by the elongated rod entering in to the phantom. The disturbance load is applied within the range 0.05–0.3 Kg. This test is particularly performed in order to replicate the sudden reaction force that may occur due to the needle–tissue interaction or hitting bones. As shown in Fig. 12(a), the robustness in performance of the system while undergoing external force disturbance at random intervals of the trajectory is observed. As the real tissue is heterogeneous in nature, different loads of 0.05 kg to 0.3 Kg are given at various destinations of the trajectory. Figure 12(b) shows its corresponding control voltage input. The controller applies corresponding voltage required to compensate the disturbance provided by the external load conditions.

As per the quantitative measure using the RMSE criterion and the disturbance overcoming capability of the APID-SMC, the control performance has been experimentally validated. The results also reinforce the fact that the active needle control toward the trajectory tracking task, will not be needing the needle–tissue interactive model.[4–9,40,56] The main outcomes of the proposed research work will be toward the possibility of exposing the active smart needle scenario into the clinical percutaneous cancerous interventions, adaptability toward dynamic environmental changes of the target and involvement of three control loops (the inner needle loop, outer robot loop and far outer physician loop) have the physician into the loop.[53]

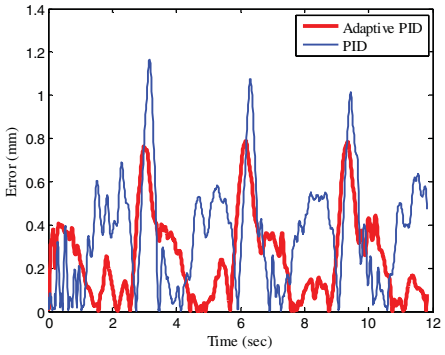
3.1. Limitations

This study presents the design and experimental evaluation of a robust adaptive PID-SMC control algorithm for steering a needle percutaneously to address therapeutic procedures. The performance

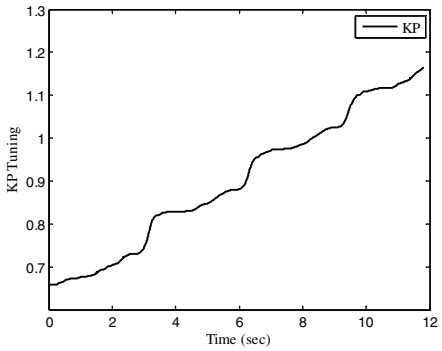
https://doi.org/10.1017/S0263574718000334 Published online by Cambridge University Press



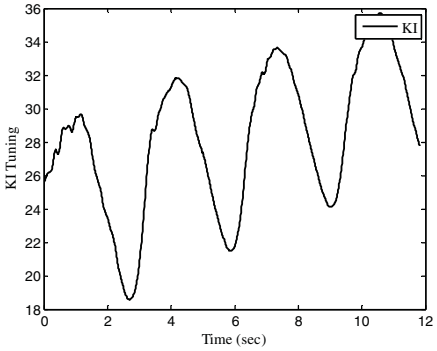
(a) Comparison of APID-SMC and PID controller in tracking the given sinusoidal reference.



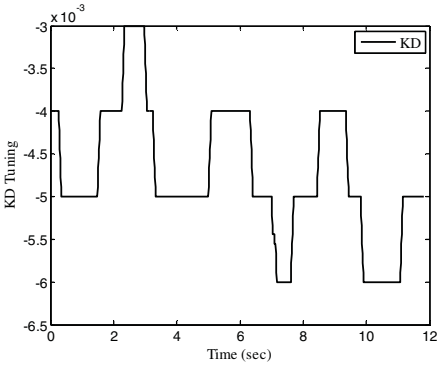
(b) Error plot



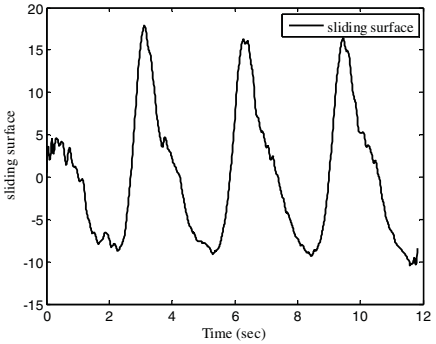
(c) Proportional gain K_P tuned adaptively



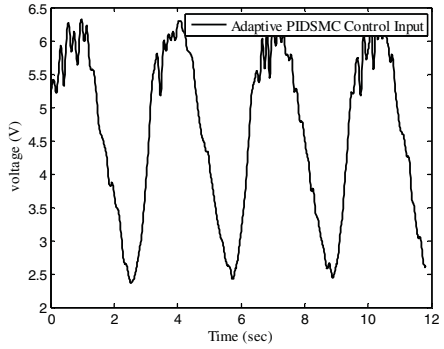
(d) Integral gain K_I gain tuned adaptively



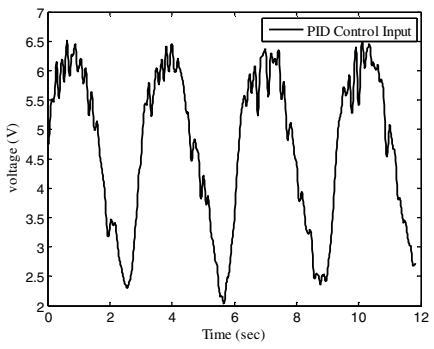
(e) Derivative gain K_D gain tuned adaptively



(f) Sliding surface



(g) APID-SMC control input voltage



(h) PID control input voltage

Fig. 8. Control performance with the given sinusoidal reference. (a) Comparison of APID-SMC and PID controller in tracking the given sinusoidal reference. (b) Error plot. (c) Proportional gain K_P tuned adaptively. (d) Integral gain K_I gain tuned adaptively. (e) Derivative gain K_D gain tuned adaptively. (f) Sliding surface. (g) APID-SMC control input voltage. (h) PID control input voltage.

https://doi.org/10.1017/S0263574718000334 Published online by Cambridge University Press

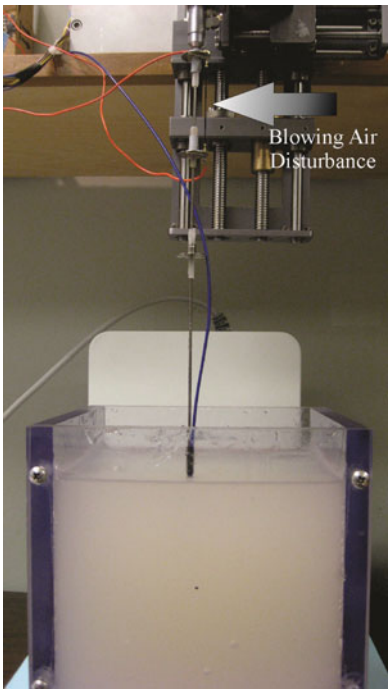
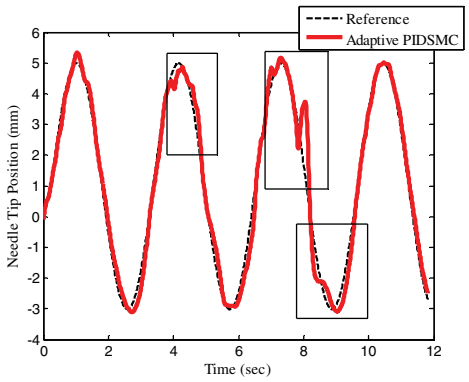
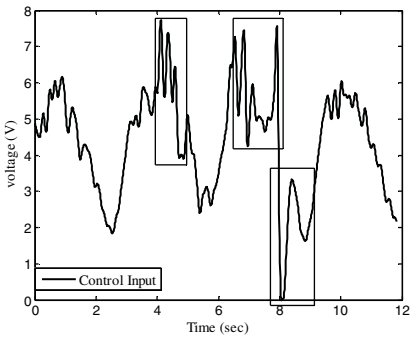


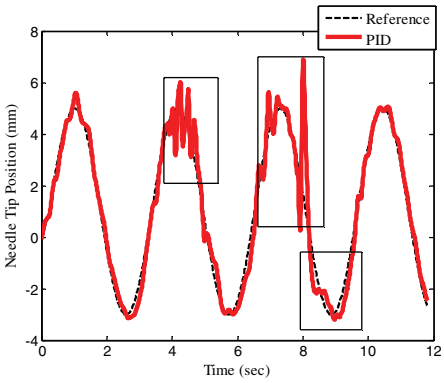
Fig. 9. External disturbance to the needle through forced convection of the SMA actuator wire by blowing air.



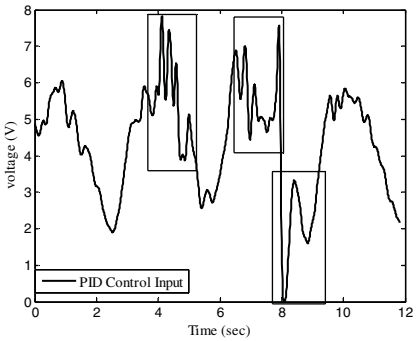
(a). Response to the reference.



(b). APIDSMC Control Input voltage.



(c). Response to the reference.



(d). PID Control Input voltage.

Fig. 10. Control performance with the given sinusoidal reference in the presence of temperature disturbance (forced convection of the SMA actuator) by blowing air on the SMA actuator at the mentioned regions. (a) Response to the reference. (b) APIDSMC control input voltage. (c) Response to the reference. (d) PID control input voltage.

https://doi.org/10.1017/S0263574718000334 Published online by Cambridge University Press

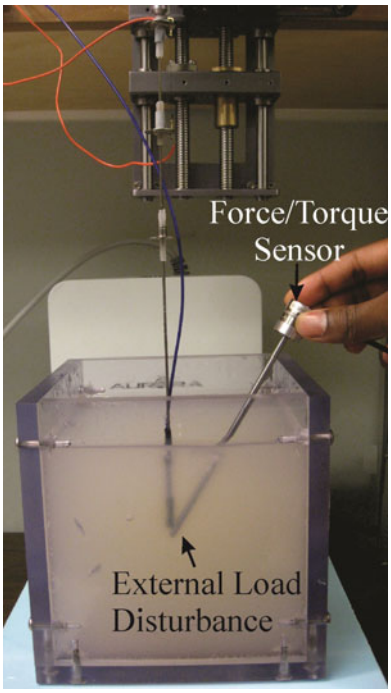
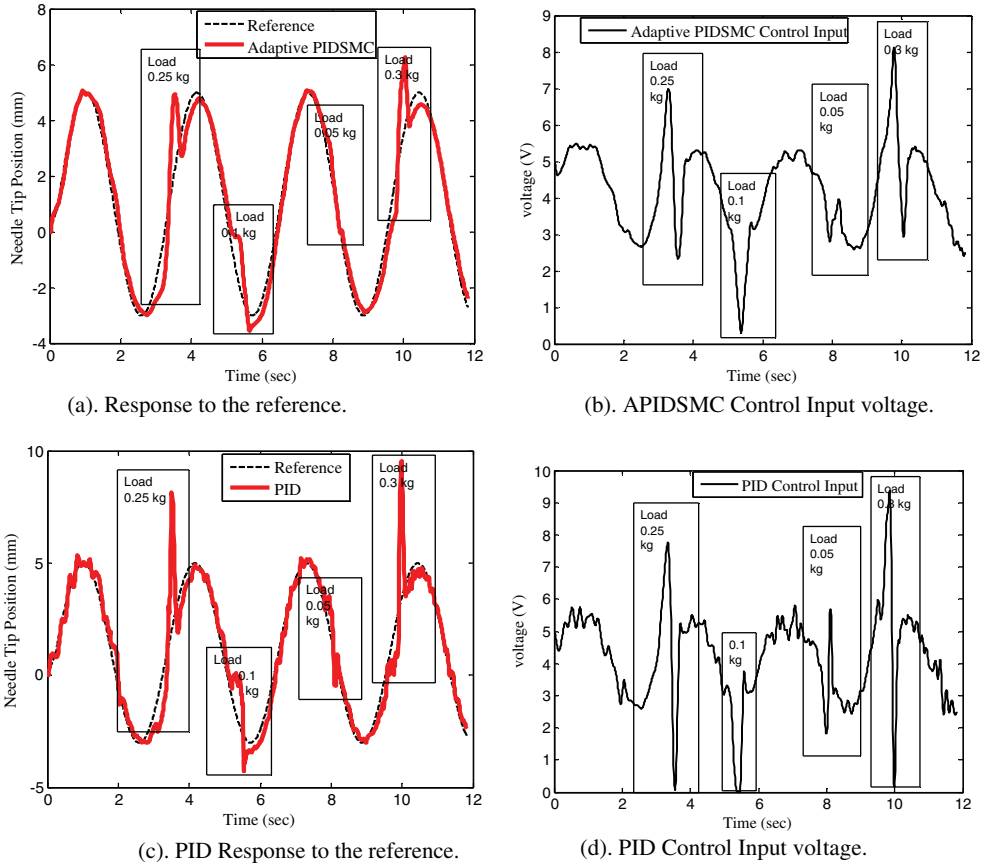


Fig. 11. External disturbance to the needle tip by applying loads in the range of (0.05 Kg to 0.3 Kg). The applied external disturbance load is measured by the force/torque sensor attached to the proximal end of the disturbing rod.



(a). Response to the reference.

(b). APIDSMC Control Input voltage.

(c). PID Response to the reference.

(d). PID Control Input voltage.

Fig. 12. APIDSMC control performance in the conditions of external force replicating the reaction force from the tissue while insertion. (a) Response to the reference. (b) APIDSMC control input voltage. (c) PID response to the reference. (d) PID control input voltage.

https://doi.org/10.1017/S0263574718000334 Published online by Cambridge University Press

has been tested using only artificial tissue phantoms, whereas the real application when the needle body is constrained in its motion by the heterogeneous biological tissues is yet to be performed and tested. In the real clinical scenario, targets are instantaneously varying due to patient breathing and motion. But, in the current study, only static target is considered. Furthermore, the test is performed using multi-step position tracking and sinusoidal trajectory tracking tasks in the tissue phantom. However, such needle tip oscillations will create critical damage to the biological tissues. Hence, we aim to involve splined precurved trajectories thereby reaching the target region by avoiding anatomical obstacles for our future study.

4. Conclusion

In this work, the APID-SMC has been deployed for the trajectory tracking control of an active SMA actuated flexible needle in artificial tissue phantom environment. Furthermore, under two disturbance analyses, first, by thermal disturbance by blowing air on the actuator and second, by applying external point load disturbances, the robustness of the applied APID-SMC is tested. From the results, it is observed that the APID-SMC is proved to be the effective method in compensating the SMA uncertainties with near clinically acceptable thresholds. The future work will involve standard and potential clinical feedback modalities such as US, MRI and CT for the closed-loop control with ex-vivo tissues.

References

1. N. Abolhassani, R. Patel and M. Moallem, "Needle insertion into soft tissue: A survey," *Med. Eng. Phys.* **29**(4), 413–431 (2007).
2. R. J. III Webster, A. M. Okamura and N. J. Cowan "Towards Active Cannulas: Miniature Snake-Like Surgical Robots," Proceedings of the IEEE/RSJ International Conference on Intelligent Robots and Systems (IROS 2006), Beijing, China, (Oct. 9–15, 2006) pp. 2857–2863.
3. P. J. Swaney, J. Burgner, R. J. Webster III and R. Alterovitz, "A flexure-based steerable needle: High curvature with reduced tissue damage," *IEEE Trans. Biomed. Eng.* **60**(4), 906–909 (2013).
4. A. M. Okamura, C. Simone and M. D. O'Leavy, "Force modeling for needle insertion into soft tissue," *IEEE Trans. Biomed. Eng.* **51**(10), 1707–1716 (2004).
5. S. P. DiMaio and S. E. Salcudean, "Interactive simulation of needle insertion models," *IEEE Trans. Robot.* **52**(7), 1167–1179 (2005).
6. O. Goksel, S. E. Salcudean and S. P. DiMaio, "3D simulation of needle-tissue interaction with application of prostate brachytherapy, *Comp. Aid. Sur.* **11**(6), 279–288 (2006).
7. D. Gao, Y. Lei, B. Lian and B. Yao, "Modeling and simulation of flexible needle insertion into soft tissue using modified local constraints," *J. Manuf. Sci. Eng.* **138**(12), 12101–12112 (2016).
8. D. Glozman and M. Shoham, "Image-guided robotic flexible needle steering," *IEEE Trans. Biomed. Eng.* **23**, 459–467 (2007).
9. A. C. Barnett, Y. S. Lee and J. Z. Moore, "Fracture mechanics model of needle cutting tissue," *J. Manuf. Sci. Eng.* **138**, 011005–011011 (2016).
10. K. B. Reed, V. Kallem, R. Alterovitz, K. Goldberg, A. Okamura and N. J. Cowan, "Integrated Planning and Image-guided Control for Planar Needle Steering," Proceedings of the Annual International Conference of the IEEE Engineering in Medicine and Biology Society, (2008) pp. 819–824.
11. K. B. Reed, A. Majewik, V. Kallem, R. Alterovitz, K. Goldberg, N. J. Cowan and A. M. Okamura, "Robot-assisted needle steering," *IEEE Robot. Autom. Mag.* **18**(4), 35–46 (2011).
12. R. Alterovitz and K. Goldberg, "The Stochastic Motion Roadmap: A Sampling Framework for Planning with Markov Motion Uncertainty," Proceedings of the Robotics: Science and Systems Conference, Atlanta, GA, USA (2007) pp. 1–8.
13. V. Kallem and N. J. Cowan, "Image guidance of flexible tip-steerable needles," *IEEE Trans. Robot.* **25**(1), 191–196 (2009).
14. J. P. Swensen and N. J. Cowan, "Torsional Dynamics of Compensation Enhances Robotic Control of Tip-steerable Needles," Proceedings of the IEEE International Conference on Robotics and Automation, Minnesota, USA (2012) pp. 1601–1606.
15. N. A. Wood, K. Shahrour, M. C. Ost and C. N. Riviere, "Needle Steering System using Duty-cycled Rotation for Percutaneous Kidney Access," Proceedings of the Annual International Conference of the IEEE Engineering in Medicine and Biology Society (2010) pp. 5432–5435.
16. N. A. Wood, K. Shehrour, M. C. Ost and C. N. Riviere "Closed-loop Control of Needle Steering for Percutaneous Kidney Access," Proceedings of the In ICRA Workshop on Snakes, Worms and Catheters: Continuum and Serpentine Robots for Minimally Invasive Surgery, 4 (2010) pp. 48–50.
17. S. Y. Ko and F. Rodriguez y Baena, "Trajectory following for a flexible probe with state/input constraints: An approach based on model predictive control," *Robot Autonomous Syst.* **60**(4), 509–521 (2012).

https://doi.org/10.1017/S0263574718000334 Published online by Cambridge University Press

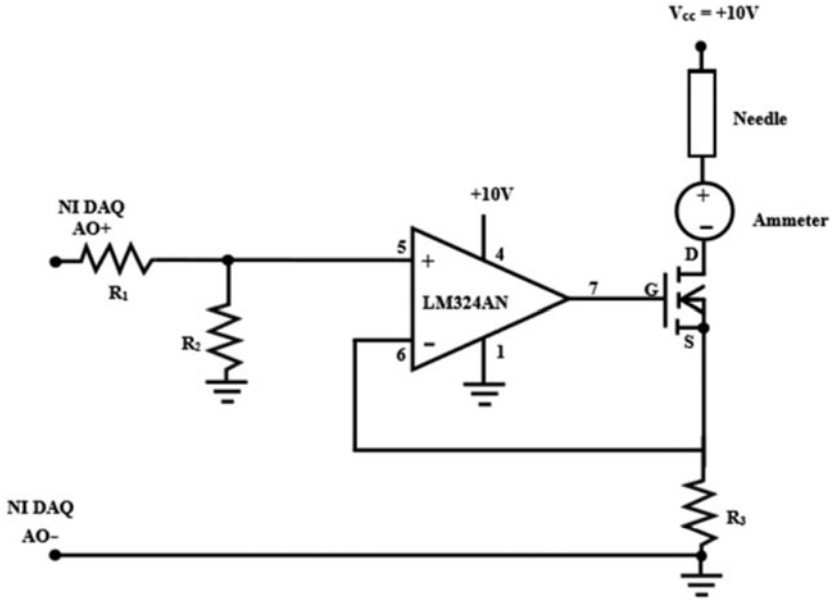
18. V. K. Bui, S. Park, J. Park and S. Y. Ko, "A novel curvature-controllable steerable needle for percutaneous intervention," *J. Eng. Med.* **230**(8), 727–738 (2016).
19. K. Hauser, R. Alterovitz, N. Chentanez, A. M. Okamura and K. Goldberg, "Feedback Control for Steering Needles Through 3D Deformable Tissue using Helical Paths," Proceedings of the in Proceedings on the Robotics: Science and Systems Conference, Seattle, USA (2009) pp. 1–8.
20. M. Abayazid, R. J. Roesthais, R. Reilink and S. Misra, "Integrating deflection models and image feedback for real-time flexible needle steering," *IEEE Trans. Robot.* **29**(2), 542–553 (2013).
21. S. Patil, J. Burgner, R. J. Webster, III and R. Alterovitz, "Needle steering in 3D via rapid replanning," *IEEE Trans. Robot.* **30**(4), 853–864 (2014).
22. T. K. Podder, P. Hutapea, K. Darvish, A. Dicker and Y. Yu, "Smart Needling System for Fully Conformal Radiation Dose Delivery in Treating Prostate Cancer," Proceedings of the ASME 2010 Conference on Smart Materials, Adaptive Structures and Intelligent Systems(SMASIS), Philadelphia, PA (Sep. 28–Oct. 1) pp. 1–4.
23. T. K. Podder, A. P. Dicker, P. Hutapea, K. Darvish and Y. Yu, "A novel curvilinear approach for prostate seed implant," *J. Med. Phys.* **39**(4), 1887–1892 (2012).
24. R. G. Stock, N. N. Stone, Y. C. Lo, N. Malhoda, J. Kao and J. K. DeWyngaert, "Postimplant dosimetry for 125I prostate implants: Definitions and factors affecting outcome," *Int. J. Radiat. Oncol. Biol. Phys.* **48**(3), 899–906 (2000).
25. R. J. Webster, J. M. Romano and N. J. Cowan, "Mechanics of precurved-tube continuum robots," *IEEE Trans. Robot.* **25**(1), 67–78 (2009).
26. P. Sears and P. Dupont, "A Steerable Needle Technology using Curved Concentric Tubes," Proceedings of the 2006 IEEE/RSJ International Conference on Intelligent Robots and Systems (IROS), Beijing, China (2006) pp. 2850–1856.
27. K. B. Reed, A. M. Okamura and N. J. Cowan, "Modeling and control of needles with torsional friction," *IEEE Trans. Biomed. Eng.* **56**(12), 2905–2916 (2009).
28. K. B. Reed, A. M. Okamura and N. J. Cowan, "Controlling a Robotically Steered Needle in the Presence of Torsional Friction," Proceedings of the IEEE International Conference on Robotics and Automation (2009) pp. 3476–3481.
29. J. P. Swensen, M. Lin, A. M. Okamura and N. J. Cowan, "Torsional dynamics of steerable needles: Modeling and fluoroscopic guidance," *IEEE Trans. Biomed. Eng.* **61**(11), 2707–2717 (2014).
30. E. C. Burdette, D. C. Rucker, P. Prakash, C. J. Diederich, J. M. Croom, C. Clarke, P. Stolka, T. Juang, E. M. Boctor and R. J. Webster, "The ACUSITT Ultrasonic Ablator: The First Steerable Needle with an Integrated Interventional Tool," Proceedings of SPIE, Med, Imag. Ultrason. Imag., Tomogr., Ther., 7629 (2010) pp. 76290V-1–79641I-10.
31. J. Burgner, P. J. Swaney, T. L. Bruns, M. S. Clark, D. C. Rucker, E. C. Burdette and R. J. Webster, "An autoclavable steerable cannula manual deployment device: Design and accuracy analysis," *J. Med. Devices* **6**(4), 041007 (2012).
32. W. J. Levy and J. J. Oro, "Curved biopsy needle for stereotactic surgery: A technical note," *Neurosurgery* **15**(1), 82–85 (1984).
33. J. Furusho, T. Ono, Y. Chiba and H. Horio, "Development of a Curved Multi-Tube (CMT) Catheter for Percutaneous Umbilical Blood Sampling and Control Methods of CMT Catheters for Solid Organs," Proceedings of the IEEE Int. Conf. Mech. Autom., (1–4, 2005) pp. 410–415.
34. F. Jelinek, R. Pessers and P. Breedveld, "DragonFlex smart steerable laparoscopic instrument," *J. Med. Devices* **8**(1), 015001–015009 (2014).
35. H. C. M. Clogenson, J. Dankelman and J. J. Van den dobbelsteen, "Steerable guidewire for magnetic resonance guided endovascular interventions," *J. Med. Devices* **8**(1), 021002–021007 (2014).
36. K. Henken, D. Van gerwen, J. Dankelman and J. J. van den dobbelsteen, "Steerable guidewire for magnetic resonance guided endovascular interventions," *Minimally Invasive Ther*. **21**(6) 408–414 (2014).
37. T. K. Adebar, J. D. Greer, P. F. Laeseke, G. L. Hwang and A. M. Okamura, "Methods for improving the curvature of steerable needles in biological tissues," *IEEE Trans. Biomed. Eng.* **63**(6), 1167–1177 (2016).
38. M. Scali, T. P. Pusch, P. Breedveld and D. Dodou, "Needle-like instrument for steering through solid organs: A review on the scientific and patent literature," *Proc. Inst. Mech. Eng. H* **231**(3), 250–265 (2017).
39. Osseon, [Online]. Available: http://www.osseon.com/osseoflex-sn-steerable-needle/.
40. A. Yamada, S. Naka, N. Nitta, S. Morikawa and T. Tani, "A loop-shaped flexible mechanism for robotic needle steering," *IEEE Robot. Autom. Lett.* **3**(2), 648–655 (2018).
41. S. C. Ryu, Z. F. Quek, P. Renaud, R. J. Black, B. Moslehi, B. L. Daniel, K. J. Cho and M. R. Cutkosky, "Design of an optically controlled MR-compatible active needle," *IEEE Trans. Robot.* **31**(1), 1–11 (2015).
42. B. Kohn, M. Honarvar and P. Hutapea, "Design optimization study of a shape memory alloy active needle for biomedical applications," *Med. Eng. Phys.* **37**(5), 469–477 (2015).
43. B. Konh, M. Honarvar and P. Hutapea, "Application of SMA wire for an active surgical needle," *ASME Paper No. SMASIS2013-3142* (2013).
44. B. Konh, N. V. Datla and P. Hutapea, "Feasibility of shape memory alloy wire actuation for an active steerable cannula," *J. Med. Device.* **9**(3), 021002-021002-11 (2015).
45. N. V. Datla, B. Kohn, M. Honarvar, T. K. Podder, A. P. Dicker, Y. Yu and P. Hutapea, "A model to predict deflection of bevel-tipped active needle advancing in soft tissue," *Med. Eng. Phys.* **36**, 285–293 (2014).

https://doi.org/10.1017/S0263574718000334 Published online by Cambridge University Press

46. N. V. Datla, J. Koo, D. Choi, B. Kohn, T. M. Nguyen, T. K. Podder, K. Darvish, A. P. Dicker, Y. Yu and P. Hutapea, "Polyacrylamide phantom for needle-tissue interaction studies with active needles," *Med. Eng. Phys.*, **36**, 140–145 (2014).
47. E. Ayvali, C. P. Liang, M. Ho, Y. Chen and J. P. Desai, "Towards a discretely actuated steerable cannula for diagnostic and therapeutic procedures," *Int. J. Robot. Res.* **31**(5), 588–603 (2012).
48. B. Ruiz, P. Hutapea, K. Darvish, A. Dicker, Y. Yu and T. K. Podder, "SMA Actuated Flexible Needle Control using EM Sensor Feedback for Prostate Brachytherapy," *IEEE-International Conference on Robotics and Automation*, Needle Steering Workshop. http://www.cs.cmu.edu/∼surgmech/NeedleWorkshop/posters/ruiz.html.
49. S. Y. Ko, L. Frasson and F. R. Baena, "Closed-loop planar motion control of a steerable probe with a "programmable bevel" inspired by nature," *IEEE Trans. Robot.* **27**(5), 970–983 (2011).
50. K. Xu, J. Zhao and X. Zheng, "Configuration comparison among kinematically optimized continuum manipulators for robotic surgeries through a single access point," *Robotica* **33**, 2025–2044 (2015).
51. F. Maria Joseph, M. Kumar, K. Franz, P. Hutapea, A. D. Dicker, Y. Z. Zhao, Y. Yu and T. Podder, "Control of shape memory alloy actuated flexible needle using multimodal sensory feedbacks," *J Autom. Control Eng.* **3**(5), 428–434 (2014).
52. F. Maria Joseph, K. Franz, Y. Luan, Y. L. Zhao, N. V. Datla, P. Hutapea, A. Dicker, Y. Yu and T. Podder, "Development of a Coordinated Controller for Robot-assisted Shape Memory Alloy Actuated Needle for Prostate Brachytherapy," Proceedings of the *36th Annual International Conference of the IEEE Engineering in Medicine and Biology Society*, Chicago, US, (Aug. 26–30, 2014) pp. 357–360.
53. F. Maria Joseph, M. Kumar, P. Hutapea, A. Dicker, Y. Yu and T. Podder, "Development of self-actuating flexible needle system for surgical procedures," *J. Med. Devices* **9**, 020945:1–2 (2015).
54. F. Maria Joseph, M. Kumar, P. Hutapea, A. Dicker, Y. Yu and T. Podder, "Closed Loop Control of a Robot Assisted Smart Flexible Needle for Percutaneous Intervention," Proceedings of the 37th Annual International Conference of the IEEE Engineering in Medicine and Biology Society, Milan, Italy (2015) pp. 3663–3666.
55. F. Maria Joseph, S. Hans, A. Singhal, A. Yadav, A. Gupta, A. Malhotra and P. S. Singh, "Inverse Kinematic Control of a Smart Active Needle for Percutaneous Intervention," Proceedings of the IEEE Region 10 Conference (TENCON), 2017, pp. 1159–1164.
56. N. J. Van de Berg, J. Dankelman and J. J. Van den Dobbelsteen, "Design of an actively controlled steerable needle with tendon actuation and FBG-based shape sensing," *Med. Eng. Phys.* **37**, 617–622 (2015).
57. D. C. Rucker, J. Das, H. B. Gilbert, P. J. Swaney, M. I. Miga, N. Sarkar and R. J. Webster III, "Sliding mode control of steerable needles," *IEEE Trans. Robot.* **29**(5), 1289–1299 (2013).
58. T. Kuo, Y. J. Huang, C. Y. Chen and Chang, C. H., "Adaptive sliding mode control with PID tuning for uncertain systems," *Eng. Lett.* **16**(3), EL_16_3_06 (2006).
59. N. T. Tai and K. K. Ahn, "Adaptive proportional-integral-derivative tuning sliding mode control for a shape memory alloy actuator," *Smart Mater. Structures* **20**, 1–13 (2011).
60. Northern Digitals: http://www.ndigital.com/products/#electromagnetic-tracking-systems
61. ATI Industrial Automation, Nano17, 6-axis Force/Torque Sensor, ATI Industrial Automation Inc., Apex, NC, 2008. [Online]. Available: http://www.ati-ia.com/products/ft/ft_models.aspx?id=Nano17.

Appendix

The power amplifier circuit for the SMA actuated active smart needle is shown below:



https://doi.org/10.1017/S0263574718000334 Published online by Cambridge University Press